

Accurate lung segmentation of thorax CT images on a tuberculosis infection model

B. Zufiria¹, L. Fernández-Terrón¹, P. Macías^{1,2}, S. Sharpe³, M. Desco^{1,2,4,5}, A. Muñoz-Barrutia^{1,2}, J.J. Vaquero^{1,2}

¹ Bioengineering and Aerospace Engineering Department, Universidad Carlos III de Madrid, Leganés, Spain, {100307044, 100316565}@alumnos.uc3m.es, {pedro.macias, manuel.desco, mariaarrate.munoz, juanjose.vaquero}@ing.uc3m.es

² Instituto de Investigación Sanitaria Gregorio Marañón, Madrid, Spain

³ Microbiology Service Division, Public Health England, Porton Down U.K sally.sharpe@phe.gov.uk

⁴ Centro de Investigación Biomédica en Red de Salud Mental (CIBERSAM), Madrid, Spain

⁵ Centro de Investigaciones Cardiovasculares Carlos III (CNIC), Madrid, Spain

Abstract

Tuberculosis (TB) remains the world's second-deadliest disease transmitted by a single infectious agent. It is urgent to develop better diagnostic tests and more effective multi-drug cocktails to improve the disease outcome. The main reservoir for these bacteria is the lungs, what makes them the most suitable location for its detection. Drug assays of new chemotherapies for treating TB require following the subjects longitudinally to assess response at several time points. In this context, the purpose of this work is to present an accurate lung segmentation algorithm for tuberculosis disease burden quantification in chest Computed Tomography (CT) scans. Building on an in-house developed lung segmentation workflow, we present and evaluate the performance of a novel algorithm able to automatically detect and extract viscera (i.e., stomach, liver, spleen) erroneously attached to the lung. Further, we evaluate the improvement on the quantification of damaged tissue obtained on the accurately segmented lungs and conclude that the refinement is relevant for the pre-clinical evaluation of the disease burden.

1. Introduction

The infection caused by *Mycobacterium tuberculosis* (MTB), which mainly affects the lungs, is one of the top 10 causes of death worldwide according to the World Health Organization [1]. Moreover, an estimated number of 480,000 people developed multidrug resistant TB (MDR-TB) [1], which increases the urgent need to develop better diagnostics test and more effective treatments.

However, the drug development pathway in TB is not completely integrated having important unanswered questions at every stage [2]. It remains unclear to what extent preclinical methods capture the right pharmacodynamics of a drug or reproduce the conditions under which it should act. Thus, developing a single drug for TB is challenging, but identifying the best drugs combination to obtain the most effective treatment regime is even harder.

In this context, High Resolution Computed Tomography (HRCT) has been employed to evaluate TB progression and response to therapy both in humans and in specific animal models, in our case, a Tuberculosis infection

model on an animal of medium size. With this aim, we have implemented a workflow that segments TB infected lungs in chest CT scans automatically [3], adapted from [4]. Further, an imaging biomarker based on the intensity differences between healthy and diseased lung parenchyma is extracted from the previously computed lung masks allowing the longitudinal evaluation of disease burden.

The anatomy of the chest in clinical and preclinical models is a challenge for automatic lung segmentation procedures. The trachea is usually included in the final segmentation although it can be deleted using some anatomical information. The same happens with some viscera in the abdominal cavity (i.e., stomach, liver, spleen) positioned below the left lung, and sometimes included in the final lung segmentation.

In this work, we present and evaluate a new algorithm, which was integrated in the above-mentioned workflow, to deal with this issue. It automatically detects the viscera, sometimes attached to the left lung, and removes it from the whole lung segmentation. Then, the goodness of the improved lung segmentation is evaluated. We also demonstrate that the parenchyma is more precisely classified as healthy and diseased (hard and soft tissue) after the refinement step.

2. Materials and Methods

2.1. CT Images

Our data consists of forty-five chest CT scans acquired from nine separate subjects at 8, 12, 16, 20 and 24 weeks after exposure to the *Mycobacterium tuberculosis* bacteria at the Microbiology Service Division of Public Health at Porton Down U.K. The subjects are separated in two different treatment groups.

2.2. Automatic Lung Segmentation Tool

Our automatic lung segmentation tool is written in Python using SimpleITK [5]. The pipeline is divided in three main steps (Figure 1): Lung segmentation, airways tree extraction and hole filling.

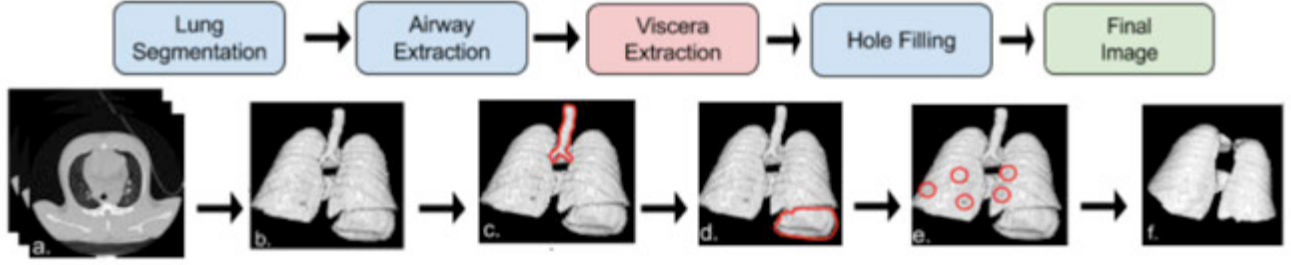


Figure 1. Workflow for the automatic lung segmentation tool: (a) Chest CT scan of the tuberculosis infected subject; (b) Segmented lung volume with the viscera attached to the left lung; (c) Trachea mask after the airway extraction step (outline in red); (d) Viscera mask after the viscera extraction step (outline in red); (e) Holes in the mask before the morphological closing step (outline in red); (f) Final mask of the infected lungs after the holes have been filled and the viscera removed.

1. *Lung Segmentation:* The air-filled structures (parenchyma and airway lumen) are isolated from the chest CT scan using an automatic adaptive thresholding combined with connectivity and topological analysis as described in [6].

2. *Airways Tree Extraction:* The trachea is automatically detected using prior information on its size and anatomical position. A seed voxel is defined on the centroid of the airways tree region located on the top-most position. From this seed position, the trachea and the rest of the main airways tree grows through the propagation of a wavefront using a three-dimensional fast marching algorithm [7]. At each step, leakage and bifurcation checks are performed until the propagation ends and the trachea and the main airways are completely segmented. Further details can be found in [8]. Once segmented, these structures are deleted from the whole lung segmentation.

3. *Hole Filling:* The algorithm described above is well suited to segment healthy lung but Tuberculosis lesions are mostly excluded. To mitigate this issue, a morphological closing operation fills the inner cavities including the damaged tissue in the lungs segmentation. An iterative hole-filling filter is applied for this morphological 3D closing.

2.3. Attached Viscera Extraction Algorithm

The main contribution of this work is the integration of an additional step in the lung segmentation algorithm workflow to perform the automatic detection and extraction of portions of viscera (most frequently stomach) retained in the lung segmented mask.

This new post-processing method is implemented in the workflow between the Airway Extraction and the Morphological Closing steps (see Figure 1 (d)). It is divided in three main processes as illustrated in Figure 2:

1. *First detection:* The viscera is detected seeking slice-by-slice, the first isolated air-filled area with a diameter in the range of 140-500 [mm] and a roundness higher than 0.8. The parameters were heuristically set.

2. *Complete selection and removal:* Starting from the first slice of viscera encountered, connected-component labelling is applied on the whole segmented volume and the detected component removed from the lung mask.

3. *Viscera and lung attachment detection:* It can happen that the procedure described in steps 1 and 2 is not enough to remove the whole attached viscera (e.g., isolated portions). To achieve the complete removal, the contours detected on previous steps are subtracted and the viscera detection is performed again on the pre-process lung mask.

2.4. Tuberculosis Infected Lungs Quantification

Our workflow incorporates a functionality to automatically compute an imaging biomarker based on the intensity differences between healthy and diseased lung parenchyma.

As described in Chen *et al.* [9], the histogram was used to define healthy and diseased-associated lung volumes, being the latter one classified in soft and hard tissue (see Figure 3).

- **Healthy volume (-1024 to -500 HU):** It corresponds to the region of the lung occupied by aerated (without visible lesions) parenchyma.
- **Soft diseased volume (-500 to -100 HU voxels):** It corresponds to lower density abnormal tissue, mainly correlated with small-to-medium nodular lesions, ground glass opacities and diffuse pulmonary infections. Soft diseased lung volume may correspond to both healing lesions and to new forming lesions.
- **Hard diseased volume (-100 to 200 HU):** It corresponds to the higher-density abnormalities (large nodular lesions, consolidations, fibrosis and bronchial thickening).

For our experiment, the thresholds were manually defined to take into account the variations in the inflation of the freely breathing animals [3]. Note that as upper threshold for the hard-diseased lung volume, 1024 HU was taken to include the densest lesions.

The imaging biomarker is the relative diseased volume defined as the ratio of the combination of hard and soft diseased volume by the total lung volume. The computed volumes at the given time points can be used to study the longitudinal evolution of the disease.

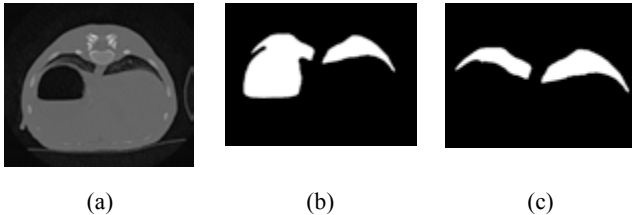


Figure 2: Illustration of the steps followed to eliminate the attached viscera: (a) Axial CT slice of one subject where the viscera can be seen attached to the left lung; (b) Lung mask obtained with the basic algorithm; (c) Refined lung mask obtained after the post-processing.

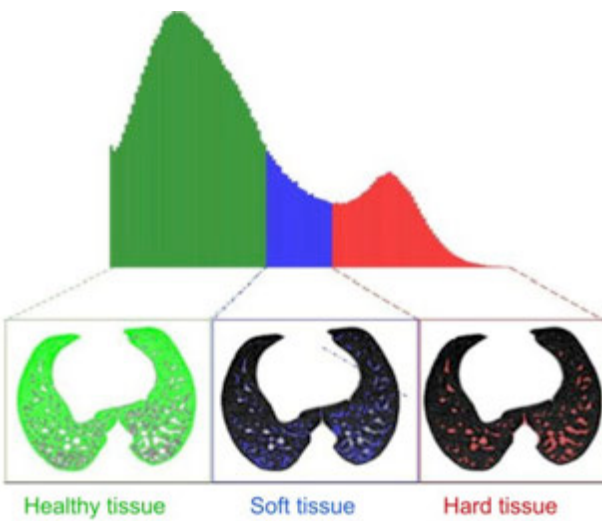


Figure 3: Manual extraction of the tuberculosis biomarker. Graphical representation of the manually defined thresholds to separate the lung histogram into three volumes: Healthy, soft diseased and hard diseased volume.

2.5. Evaluation of the Viscera Extraction

To evaluate the performance of the attached viscera extraction algorithm, the filled-with-air viscera close to the left lung were annotated on all the volumes.

Then, the Dice Similarity Coefficient (DSC) defined as

$$DSC = \frac{2 \cdot |A \cap B|}{|A| + |B|}$$

(where A and B correspond to each of the mask to compare) was obtained using two different sets of masks as inputs.

We first compare the manual viscera and the lung mask obtained with the refinement algorithm. In this case, we expect DSC values close to zero, because after the viscera extraction step, the masks should not overlap.

Then, we compare the overlap between the refined lung mask and the original lung mask from which the manually annotated viscera has been removed. With this experiment, we aim to demonstrate that the refined segmentation correctly delineates the lungs. In this case, we expect the recovered DSC values to be close to one.

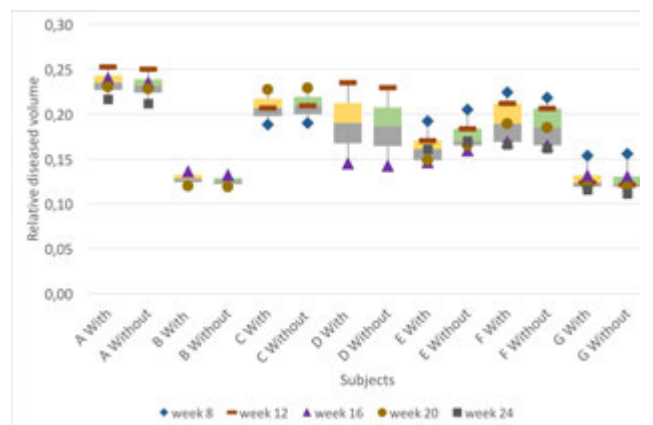


Figure 4: Box plots of the relative diseased volume per subject measured before (shown in yellow) and after the viscera extraction step (shown in green).

The Hausdorff distance (HD) and the Hausdorff distance averaged (HDA) were also computed on this dataset. The HD represents the maximum distance between two segmented surfaces and it is defined as:

$$HD = \max(\max_{s_a \in S(A)} d(s_a, S(B)), \max_{s_b \in S(B)} d(s_b, S(A))),$$

where s_a and s_b represent the points in the surfaces of A and B, $S(A)$ and $S(B)$ the set of all the points in the surfaces of A and B, respectively, and d the Euclidean distance. This measure is very sensitive to outliers.

The HDA is computed as the average of all the distances between surfaces and consequently, gives a global idea of how similar the topologies of both surfaces are.

3. Results

3.1. Evaluation of the Viscera Extraction

When measuring the overlap between the manual viscera annotation and the mask computed using the improved algorithm, the DSC is 0.014 ± 0.017 .

While the overlap between the refined lung mask and the original mask from which the manually annotated viscera has been removed, the DSC is 0.991 ± 0.005 . The HD is 14.5 ± 8.406 and the HAD, 0.016 ± 0.019 , both measures are given in millimetres.

The results of the evaluation demonstrate that the novel post-processing step is working properly. The low DSC value in the first comparison means that the viscera portion kept in the lungs mask is residual. However, when comparing clean lungs (second case), we obtain nearly perfect overlap of the lung masks.

This result is supported by the small value of the HAD indicating a good concordance of the surfaces topologies. Note that the relatively high value of the mean HD is due to a faulty viscera extraction in a limited number of slices as demonstrated by the large standard deviation.

3.2. Improvement in the Quantification of the Diseased Lung Volume

After the post-processing, for all the selected cases, the volume of the lung mask decreases as the erroneously included viscera has been mostly removed. In particular, the total volume of healthy and diseased tissue gets reduced (data not shown). Moreover, the differences between the total healthy and diseased lung volumes before and after the refinement step are statistically significant (t-test, p-value<0.001).

However, referring to relative volumes, in most of the patients, the relative diseased volume tends to decrease as can be observed in Figure 4. Correspondingly, the relative healthy volume tends to increase as both (relative diseased and healthy) sums up to one. Nevertheless, the differences are not statistically significant as it is the case for the total volumes.

4. Conclusions

We have proposed a viscera extraction algorithm that has been integrated in our lung segmentation workflow. Namely, it remains fully automatic and the detection of the attached viscera is based on some a prior information of their location and size.

The post-processing algorithm has been proved to work properly, eliminating the viscera attached to the left lung, as demonstrated by the performed evaluations that just give a residual volume overlap between the annotated viscera and the refined lung masks. The maximal distance between the surfaces is not negligible, pointing out to some local errors of the post-processing. In other words, the HD is very sensitive to outliers. So, when a small portion of the viscera is not completely removed by the post-processing, it generates considerably large HD values. Fortunately, the average distances are very small indicating a global good performance of the algorithm.

The volumetric data of the original lung segmentations (with part of the viscera included) are largely distorted. Namely, the total, healthy and diseased lung volumes have an error that it is impossible to predict. With the attached viscera extraction algorithm implemented in the automatic segmentation tool, we reduced the total volume just focusing on the lungs obtaining more precise results.

This further changes the relative lung volumes measures. Observing the relative healthy and diseased lung volumes, as the latter shows a decreasing trend, the healthy has the opposite behaviour. This means that the lung segmentation workflow without the improvement includes part of the false positive volume as healthy tissue and another random part as diseased. Consequently, the lung segmentation without including the viscera allows obtaining a more realistic longitudinal evolution of the disease and ultimately, a more precise assessment of treatment response.

Acknowledgements

The research leading to these results was supported by funding from the Innovative Medicines Initiative Joint

Undertaking under grant agreement nº 115337, the resources of which comprise financial contributions from the European Union's Seventh Framework Program (FP7/2007-2013) and EFPIA companies ('in kind contribution'). This work was also partially funded by the projects TEC2013-48552-C2-1-R, TEC2014-56600-R, RTC-2015-3772-1, TEC2015-73064-EXP and TEC2016-78052-R from the Ministry of Economy, Industry and Competitiveness (MEIC). The CNIC is supported by MEIC and the Pro CNIC Foundation, and is a Severo Ochoa Center of Excellence (SEV-2015-0505).

References

- [1] World Health Organization (WHO) official webpage. <http://www.who.int/mediacentre/factsheets/fs104/en/> (Accessed: 11-Jul-2016).
- [2] PreDiCT-TB project webpage. <http://www.predict-tb.eu/> (accessed 29-Sept-2019).
- [3] Muñoz-Hernando M, Macias P, Abella M, Desco M, Sharpe S, Vaquero J.J., Muñoz-Barrutia A. Preliminary Evaluation of a Radiological Biomarker to Characterize the Longitudinal Evolution of Tuberculosis. Libro de Actas del XXXIV Congreso Anual de la Sociedad Española de Ingeniería Biomédica (CASEIB'16), 2016.
- [4] Artaechevarria X, Blanco D, de Biurrun G, Ceresa M, Perez-Martin D, Bastarrika G, de Torres JP, Zulueta JJ, Montuenga LM, Ortiz-de-Solorzano C, Muñoz-Barrutia A. Evaluation of micro-CT for emphysema assessment in mice: comparison with non-radiological techniques, Eur Rad, vol. 21, n. 5, pp. 954-962, 2011.
- [5] Lowekamp BC, Chen DT, Ibáñez L and Blezek D (2013) The Design of SimpleITK. *Front. Neuroinform.* 7:45. doi: 10.3389/fninf.2013.00045
- [6] Hu S, Hoffman E, Reinhardt J. Automatic lung segmentation for accurate quantification of volumetric x-ray CT images. *IEEE Trans Med Imaging*, vol. 20, 2001, pp. 490-498.
- [7] Schlathoelter T, Lorenz C, Carlsen IC, et al. Simultaneous segmentation and tree reconstruction of the airways for virtual bronchoscopy. *Proc SPIE*, vol. 4684, 2002, pp. 103-113.
- [8] Artaechevarria X, Perez-Martin D, Ceresa M, de Biurrun G, Blanco D, Montuenga LM, van Ginneken B, Ortiz-de-Solorzano C, Muñoz-Barrutia A. Airway segmentation and analysis for the study of mouse models of lung disease using micro-CT, *Phys Med Biol*, vol. 54, n. 22, pp. 7009, 2009.
- [9] Chen RY, Dodd LE, Lee M, Paripati P, Hammoud DA, Mountz JM, Jeon D, Zia N, Zahiri H, Coleman MT et al. PET/CT imaging correlates with treatment outcome in patients with multidrug-resistant tuberculosis. *Science translational medicine*, vol.6, no. 265, 2014, pp.265ra166